Elsevier Editorial System(tm) for Engineering Structures
Manuscript Draft

Manuscript Number:

Title: BUCKLING MODELING OF REINFORCING BARS WITH IMPERFECTIONS

Article Type: Research Paper

Keywords: reinforcing bar; buckling; reinforced concrete; model

Corresponding Author: Dr. Leonardo M Massone, Ph. D.

Corresponding Author's Institution: University of Chile

First Author: Leonardo M Massone, Ph. D.

Order of Authors: Leonardo M Massone, Ph. D.; Daniel Moroder

Abstract: Reinforced concrete columns in seismic zones are subjected to combined actions, resulting in axial loads in longitudinal reinforcing bars. Thus, knowing the bar response, especially when it is subjected to important axial compressive forces that might lead to buckling, is important. A bar buckling model based on concentrated plasticity and with the capability of introducing an initial imperfection is described. Additionally, a comprehensive study of the monotonic tensile response beyond the peak stress point and a simple cyclic rule, complete the physical approach of the model. Comparisons of the model with experimental results reveal that peak capacity (average axial stress) is well captured, as well as the post-peak response shape (average axial stress versus strain), with differences observed basically in the peak capacity for specimens with high bar imperfection-to-diameter ratio, and in the shape of the post-peak response for specimens with low bar length-to-diameter ratio.

Suggested Reviewers: Juan F Beltran Ph.D.
Assistant Profesor, Civil Engineering, University of Chile
jbeltran@ing.uchile.cl
Prof. Beltran is a co-worker interested in the topic.

Kutay Orakcal Ph.D.

Assitant Profesor, Civil Engineering, Boğaziçi University
kutay.orakcal@boun.edu.tr
Prof. Orakcal is in structural and earthquake engineering with emphasis in reinforced concrete testing and modeling.

BUCKLING MODELING OF REINFORCING BARS WITH IMPERFECTIONS

Leonardo M. Massone[1], and Daniel Moroder[2]

ABSTRACT

Reinforced concrete columns in seismic zones are subjected to combined actions, resulting in axial loads in longitudinal reinforcing bars. Thus, knowing the bar response, especially when it is subjected to important axial compressive forces that might lead to buckling, is important. A bar buckling model based on concentrated plasticity and with the capability of introducing an initial imperfection is described. The initial imperfection is imposed by bending the bar with a transversely applied nonpermanent force. Additionally, a comprehensive study of the monotonic tensile response beyond the peak stress point and a simple cyclic rule, complete the physical approach of the model. Comparisons of the model with experimental results reveal that peak capacity (average axial stress) is well captured, as well as the post-peak response shape (average axial stress versus strain), with differences observed basically in the peak capacity for specimens with high bar imperfection-to-diameter ratio, and in the shape of the post-peak response for specimens with low bar length-to-diameter ratio.

Keywords: reinforcing bar; buckling; reinforced concrete; model

[1]Assistant Professor, Department of Civil Engineering, University of Chile, Blanco Encalada 2002, Santiago, Chile
[2]Master student in Civil Engineering, University of Bologna, Viale Risorgimento 2, 40136, Bologna, Italy

1. INTRODUCTION

Reinforced concrete columns in seismic zones are subjected to combined actions that include mainly axial, moment and shear forces. Longitudinal reinforcing bars act as members that resist axial loads, which also contributed to maintain the moment of the column. Thus, the axial response of longitudinal bar becomes relevant. In absence of buckling effects the axial response can be associated to the monotonic or cyclic response of bars. That situation, although ideal, might not represent all cases. Reinforced concrete columns under cyclic lateral displacements, which represent a seismic action, would remain elastic under small displacements. Under severe loading, lateral displacements would increase, and in combination with compressive axial forces, deterioration of cover concrete that ends with spalling would reveal part of the longitudinal bars which are supported by stirrups. A large distance between stirrups would trigger buckling at lower loads, which also affects the column response. Thus, modeling of buckling is required to establish a good understanding of column behavior, especially when the longitudinal bar response may be affected by relatively large stirrup separation.

The study of buckling has its beginning with Euler in the 18th century, which developed a simple equation to calculate the critical load for the elastic case. More recent developments have included material inelasticity. The application to reinforced concrete modeling appeared with Bresler and Gilbert [**1**], providing the information about tie spacing requirements and the buckling behavior of longitudinal reinforcement steel in compressed concrete members based on critical load estimation at yielding. Further efforts

have been done by researchers in order to capture not only the buckling capacity of longitudinal bars, but also to describe their monotonic, as well as their axial cyclic response. Numerical simulations using fiber discretization of beam-column elements with distributed plasticity have been introduced (e.g., Mau and El-Mabsout [**2**]; Dhakal and Maekawa [**3**]), characterizing in part the monotonic response. Cyclic response has also been estimated based on calibration of monotonic experimental response of bars subjected to buckling (e.g., Dhakal and Maekawa [**3**]; Monti and Nuti [**4**]), allowing the introduction of cyclic constitutive material laws for steel including buckling into beam and column analysis. Other authors have adopted different modeling approaches to introduce the buckling behavior to the beam and columns responses, such as introducing concentrated plasticity models based on steel material constitutive laws (e.g., Gomes and Appleton [**5**]; Restrepo [**6**]).

2. RESEARCH SIGNIFICANCE

The model describe in this paper considers a similar approach adopted by Restrepo [**6**] but with the capability of introducing an initial imperfection, imposed by bending the bar with a transversely applied nonpermanent force. Additionally, a comprehensive study of the monotonic response pointed out the need of defining the tensile response beyond the peak stress point, and a consistent point of fracture. Altogether, with a reliable compressive constitutive law for the steel material and a simple cyclic rule, helps to an overall simple and physical approach to the problem. Thus, this model, verified with experimental tests from the literature, can be implemented into column analysis.

3. MODELING STUDIES

3.1 Tensile material model

Common mild reinforcing steel bars are usually characterized by their monotonic stress versus strain response in tension. The tensile monotonic response of bars behaves linear-elastic until yielding is achieved (f_y, ε_y in **Fig. 1**), maintaining an almost constant stress until initiation of strain hardening is observed (f_y, ε_{sh} in **Fig. 1**). Different steel composition may result in a softer tensile response, showing a curved transition from the linear-elastic zone to the strain hardening zone. Strain hardening is understood as an increase of strength with the increment of strain. The peak strength, or maximum strength (f_m, ε_m in **Fig. 1**), is followed by a degradation of the strength, which is also associated to a strain localization that results in a local cross-section reduction at weaker zones of the bar. Ultimate strength (f_u, ε_u in **Fig. 1**) is observed before the axial strength drops to zero at the onset of bar fracture. **Figure 1** shows a representation of the overall stress versus strain response of reinforcing bars in tension characterized by the model proposed by Mander et al. [**7**]. The model by Mander presents an elasto-plastic response until reaching the initiation of hardening (f_y, ε_{sh} in **Fig. 1**), followed by a curve that describes the hardening range until the peak strength point (f_m, ε_m in **Fig. 1**). The degrading zone, not characterized by Mander, and usually by no one for engineering purposes, is assumed linear until bar fracture (f_u, ε_u in **Fig. 1**). The experimental determination of the constitutive monotonic material response for steel in tension once strain localization begins (at peak strength) is spurious due to the fact that the strain concentration might fall inside or outside the gage length of the instrument

measuring axial deformation, resulting in either larger or smaller deformations, respectively. Not only that, even if the concentration of deformation is guarantied to be localized inside the instrumented length, the experimental stress-strain response would be associated to the gauge length used for deformation measurement. That is, if the strain concentration is distributed over a length, l_p, which is smaller than the gauge length, l_g, the engineering strain, measured over the gauge length would result in a smaller strain (**Fig. 2**). In general, if a section of the longitudinal bars under axial load presents strain concentration due to softening of the material, i.e. larger strain at lower stress, all other points in the bar in order to maintain equilibrium, as a beam-column element, are required to unload instead of overcome the peak stress. In **Fig. 2**, a scheme of a reinforcing bar undergoing tensile forces is shown assuming that the strain concentration zone falls inside the displacement transducer length used to determine the bar strain. The zone with strain concentration over the length l_p reveals the actual material constitutive stress versus strain response in engineering coordinates, where after reaching the peak strength (point 1) continues straining until point 2. Outside the strain concentration zone, after reaching the peak strength (point 1) instead of continue straining, undergoes unloading (point 2) due to material heterogeneity that results in slightly stronger sections. In terms of the overall response, using a displacement transducer over a length l_g (larger than the strain localization zone) to determine the bar relative displacement, and then the average strain, results in smaller strain values after the peak stress than at the strain localization zone. Thus, the ultimate strain defined for the strain concentration zone, $\varepsilon_{u,p}$, is determined by

$$\varepsilon_{u,p} = \varepsilon_m + \left[\left(\varepsilon_{u,g} - \varepsilon_m \right) \cdot l_g + \left(\frac{f_u - f_m}{E_s} \right) \cdot \left(l_g - l_p \right) \right] \Big/ l_p \qquad (1)$$

where $\varepsilon_{u,g}$ is the ultimate strain based on the gauge length, and under the assumption that the unloading response follows the initial elastic stiffness, E_s. Common mild reinforcing steel bars present large ultimate strain, which leads to the approximation of Eq. (**1**) given by

$$\varepsilon_{u,p} \approx \varepsilon_m + \left(\varepsilon_{u,g} - \varepsilon_m\right) \cdot \frac{l_g}{l_p} \tag{2}$$

The previous equations determine the real strain at the strain concentration zone by correcting the strain values obtained experimentally after the peak stress was reached, under the assumption that the strain concentration falls inside the gauge length.

In general, constitutive material models for reinforcing bars have been calibrated using data before degradation is observed (e.g., Mander et al. [**7**]) to avoid spurious results. Also, many analyses would not require reaching such large strains. The model verification presented in this study requires in some cases reaching large tensile strains, which forces the analysis to calibrate the tensile response of reinforcing bars after reaching the peak stress.

3.2 Compressive material model

The tensile stress versus strain response is usually also adopted as the response for the steel in compression. However, it has been shown that the use of engineering coordinates to estimate the stress and the strain as well, that is using the initial cross-sectional area and bar length to estimate such magnitudes, does not represent the true or actual stress or strain the material is undergoing due to sequential increase of element length and decrement of cross-sectional area while in tension. The use of true coordinates or natural coordinates as

indicated by Dodd and Restrepo-Posada [**8**] provides stress and strain measurement accounting for the current cross-sectional area and bar length. These stress and strain measurement has been shown to provide a good estimate for the stress versus strain response for bars in compression, assuming an identical behavior of the steel material in tension and compression in true coordinates. Thus, compressive response can be estimated from tensile tests. According to Dodd and Restrepo-Posada [**8**] findings such analysis gives good correlation with tests results performed in compression until buckling is observed. The compressive stress versus strain response ($f_{s,c}$, $\varepsilon_{s,c}$) can be determined by

$$f_{s,c} = -f_{s,t}\left(1+\varepsilon_{s,t}\right)^2 \tag{3}$$

$$\varepsilon_{s,c} = -\frac{\varepsilon_{s,t}}{1+\varepsilon_{s,t}} \tag{4}$$

where $f_{s,c}$ and $\varepsilon_{s,c}$ are the stress and strain coordinates (engineering coordinates) in compression (negative) for the corresponding stress, $f_{s,t}$, and strain, $\varepsilon_{s,t}$, coordinates (engineering coordinates) in tension (positive). Thus, once the constitutive steel material response is characterized in tension through tests, and the post-peak is corrected in order to represent the strain values in the strain concentration zone, Eq. (**3**) and (**4**) can be used to determine the compressive constitutive steel response. Although, tensile tests end with bar fracture, that ultimate point value may not be consistent with a failure mechanism in compression when using Eq. (**3**) and (**4**). Post-peak points for the tensile response can be extrapolated assuming no fracture failure in order to estimate the compressive response.

3.3 Simple cyclic material model

The previous analysis defines the monotonic behavior of steel reinforcement. Cyclic response requires more detailed description. Many steel constitutive material models have been proposed to predict cyclic response (e.g., Menegotto and Pinto [**9**]; Dodd and Restrepo-Posada [**8**]; Mander et al. [**7**]), although most of them have assumed identical compressive and tensile response of steel. Such assumption is reasonable for relative small strain values. However, the analysis of bars that present buckling with an initial imperfection shows relative high axial strain even for the first loading steps (e.g., induction of the initial imperfection imposed by bending the bar with a transversely applied nonpermanent force at bar midheight). For the analysis of reinforcing bar buckling under monotonic axial loading, cyclic response of steel is required in order to describe initial imperfections or model deviation from a uniform strain distribution in the cross-section once buckling is onset. In this case, usually no full cycles are achieved. Thus, a calibrated material model, capable of reproducing few or incomplete cycles, for not only small strains, but also relatively large strains is required to capture the response of buckling bars that consider imperfections.

The suggested simple cyclic material model for steel is depicted in **Fig. 3**. The model maintains both envelop monotonic responses for steel in tension and compression. Once reversal loading occurs from the envelope (e.g., $f_{r,1}^{-}$, $\varepsilon_{r,1}^{-}$ or $f_{r,1}^{+}$, $\varepsilon_{r,1}^{+}$ in **Fig. 3**) outside the linear range a curve (called curve *A*) joints the current unloading point (origin) and a point with the same strain coordinate of the previous unloading point from the opposite envelope

(end). The end stress of curve *A* is determined based on the assumption that straining in one direction shifts the origin of the opposite envelop curve (dashed lines). The shifted envelop curve, that is connected with an elastic stiffness to the unloading point, starts from a virtual plastic strain point (e.g., point (0, $\varepsilon_{p,1}^{+}$) in **Fig. 3**) and defines the new stress value. In case of unloading from the envelope for the first time, the zero strain point in the opposite envelope is selected as the previous unloading point in that branch. After following the curve *A*, it is considered for simplicity that the material model follows the remaining envelope curve (initiation or connection to the envelope curve is marked with a dot in **Fig. 3**). In the linear range, i.e., before yielding, the response is maintained within the linear-elastic behavior. In case of unloading or reloading within a curve *A*, a similar curve can be defined that joints reversal from curve *A* to the previous unloading point from the opposite envelope or another unloading point from curve *A*. For the purposes of this study, it is considered that unloading or reloading within a curve *A* are forced to joint to the previous point from the opposite envelope, maintaining the same model parameters for curve *A*.

The curve *A* represents the Bauschinger effect, that is, softer unloading and reloading branches affected by the strain previously attained. Chang and Mander [**10**] present a formulation to characterize curve *A*, based on the Menegotto-Pinto equation, which allows defining, among others, the initial and final unloading/reloading stiffness values. Although this formulation is general, it presents the disadvantage of requiring a numerical iterative scheme in order to connect initial and end points of curve *A*. Such formulation is simplified in this study by adopting a final unloading/reloading stiffness value that guarantees

connecting the initial and end points of curve *A*. The modified stress (f_s) versus strain (ε_s) expression that characterize curve *A* is given by

$$f_s = f_o + E_o\left(\varepsilon_s - \varepsilon_o\right)\left\{Q + \frac{1-Q}{\left(1+\left[E_o\left(\frac{\varepsilon_s-\varepsilon_o}{f_f-f_o}\right)\right]^R\right)^{1/R}}\right\} \tag{5}$$

where R is a parameter that represents the Bauschinger effect, E_o is the initial unloading/reloading modulus of the steel bar, f_o and ε_o are the stress and strain coordinates of the origin of curve *A*, f_f and ε_f are the stress and strain coordinates of the end of curve *A*, and Q is a parameter defined as $Q = \frac{E_{\text{sec}}/E_o - a}{1-a}$ (with $E_{\text{sec}} = \frac{f_f - f_o}{\varepsilon_f - \varepsilon_o}$ and $a = \left(1+\left[E_o/E_{\text{sec}}\right]^R\right)^{-1/R}$) that warranties that curve *A* ends at (ε_f, f_f). Equation 5 describes a function that connects the origin and end points by means of a variable radius of curvature (R), such that small values of R result in a soft transition between an initial stiffness Eo, and a final stiffness. In the other hand, large values of R (e.g., 25) results in a curve that closely follows two asymptotes formed by the initial and final stiffness, that is, instead of gradually changing the slope, curve *A* presents a kink characterized by two slopes (the initial and final stiffness values). The previous function is then fully known after defining the parameter R and the stiffness E_o. According to the cyclic formulation by Chang and Mander [**10**] and after calibration with experimental data of tests performed by Panthaki (1991) (reported by Chang and Mander [**10**]), these parameters for unloading branch are

$$E_o = E_s\left(1-3\Delta\varepsilon\right) \tag{6}$$

$$R = 16\left(\frac{f_y}{E_s}\right)^{1/3}\left(1-10\Delta\varepsilon\right) \tag{7}$$

and for the reloading branch

$$E_o = E_s\left(1-\Delta\varepsilon\right) \tag{8}$$

$$R = 20\left(\frac{f_y}{E_s}\right)^{1/3}\left(1-20\Delta\varepsilon\right) \tag{9}$$

where $\Delta\varepsilon = \left|\varepsilon_f - \varepsilon_o\right|/2$, and f_y and E_s represent the yield stress and elastic stiffness of the steel bar.

In order to verify good correlation between the proposed cyclic model and experimental results a series of data reported by Chang and Mander [**10**] are used. Representative results are presented in **Fig. 4**. As it can be seen, the general trend is captured with this simple model. However, slope discontinuities are expected in transition zones from curve *A* to the monotonic envelop as observed in **Fig. 4(a)** and **4(c)**.

3.4 Lumped plasticity buckling model for reinforcing bar

Reinforced concrete columns are commonly constructed as a series of longitudinal bars supported by stirrups or cross-ties surrounded by concrete, which are design to withstand axial (usually compressive loads), moment and shear forces. The following discussion focuses on axial and moment action on columns. Such actions transfer axial forces to the longitudinal reinforcement together with transversal forces from concrete core (inside

stirrups) expansion and stirrup straining. The axial forces in compression on reinforcing bars may lead to buckling between two consecutive stirrups (**Fig. 5**). This behavior has been capture by many researchers (e.g., Bayrak and Sheikh [**11**]; Bae et al. [**12**]) considering variables such as bar diameter, stirrup spacing, as well as an initial imperfection that deviates the bar from being straight.

In order to capture not only the bar critical load, that is, the load required to buckle the bar, but also the overall stress versus strain response, a sufficiently refined model is required. The model described in this study was adapted from Restrepo [**6**] to incorporate an initial imperfection, and was compared to experimental results available in the literature (reflecting the conditions imposed in the experiments).

The model for a bar of diameter d and length L between two consecutive stirrups assumes fixed condition at both ends, with the exception of the upper end, which is allowed to move vertically (longitudinally, see **Fig. 5**). The initial imperfection, e, is included as a transversal deviation from the vertical axis. All deformations are concentrated in four plastic hinges located at both ends and at both sides of the mid-length of the bar. The selection of the location of the plastic hinges obeys to the nature of the loading conditions. For the selected specimens the imperfection is obtained after clamping both ends and applying a transversal point load at bar mid-length, resulting in maximum moments at bar ends and mid-length. Assuming uniform material properties along the bar, the zone of maximum moment would result in concentration of deformation once linear behavior is overcome. The symmetry of the load application leads to the conclusion that the

concentration of deformation at bar mid-length can be divided into two plastic hinges. After the imperfection is included, the progression of the axial load would deform the bar even further, but in this case the axial load would result in a constant vertical force along the length of the bar and a moment distribution similar to what is expected while inducing the imperfection. Thus, if axial strain and curvature are concentrated only inside the plastic hinge length, inducing the imperfection as well as the posterior application of the axial load results in the same four hinge configuration. The aforementioned plastic hinge formulation does not satisfy the beam solution within the linear elastic range since it assumes that there are always four hinges with same moment and rotation, which is not consistent when loading the bar to induce the imperfection while the material model remains elastic. Although this approximation, it is shown in a later section, by comparing the response of the analytical model to experimental results, that the overall average stress versus strain response is captured, including the peak stress and post-peak curve shape.

At this point, once the axial strain and curvature values are known, a sectional analysis would allow determining the axial stresses at different location of the bar cross-section under the Bernoulli's hypothesis (plane sections remain plane after rotation), and using the uniaxial material constitutive law. Axial resultant force and resultant moment are determined based on integration of the uniaxial stresses and tributary areas.

3.4.1 Initial imperfection

The initial imperfection, e, can be approximately imposed by forcing a uniform curvature, ϕ_e, over the plastic hinge length, l_p, equal to

$$\phi_e = \tan^{-1}\left(\frac{e}{L/2 - l_p}\right) \Big/ l_p \tag{10}$$

Imposing an initial curvature over the plastic hinge length would result in permanent resultant moment at the plastic hinges. In order to satisfy equilibrium at the initiation of the axial tests, that is, all resultant moments need to become zero since there is no longer a transversal force inducing the imperfection. This suggests that the initial imposed curvature needs to be reduced in order to observe unloading at different points in the cross-section that results in zero resultant moment. After unloading, the residual curvature becomes ϕ_e, which yield to a permanent transversal displacement e. Giving the relatively high unloading stiffness, small variation of curvature is anticipated and the imperfection value would vary in many cases slightly after unloading. It can be numerically solved for the initial curvature required to obtain the desirable imperfection e.

The described procedure assumes that the impact of the axial strain is small. If axial strain of the plastic hinge is measured at the bar centroid, differences in the tensile and compressive envelop stress versus strain responses would result in relatively small axial strains. Similar phenomenon is anticipated when the curvature is reduced due to unloading. Preliminary analysis suggests that incorporating the axial flexibility results in small differences.

3.4.2 Application of axial force

The application of the axial force, p, changes the previous equilibrium, modifying the axial strain, ε, and curvature, ϕ, in the plastic hinge zone. At the cross-section level (**Fig. 6**), the uniaxial strain at fiber i at a distance x_i from the centroid (reference), ε_i, would vary assuming the Bernoulli's hypothesis by

$$\varepsilon_i = \varepsilon + \phi x_i \tag{11}$$

The uniaxial cyclic constitutive material model is used to determined the stresses, σ_i, at each fiber i. The resultant force (p) and moment (m) are determined by

$$p = -\sum_i \sigma_i A_i \tag{12}$$

$$m = \sum_i \sigma_i A_i x_i \tag{13}$$

where A_i is the tributary area of each fiber i.

Therefore, the application of the axial force induces a moment resultant at the plastic hinge. The symmetry of the problem under study allows analyzing only one quarter of the bar that stands in between two consecutive stirrups. **Fig 7** shows the element under analysis. The upper end of the selected segment of the bar (quarter) falls in the inflection point, resulting in no moment, but just axial force. The other end, however, has a resultant moment m. From equilibrium

$$m = p\frac{(e+w)}{2} \tag{14}$$

where w is the additional transverse displacement at bar mid-length. The transverse displacement is determined based on the geometry of the deformation mechanism assuming that all transversal deformations appear after rotation of the plastic hinges. The total transverse displacement at mid-length can be determined by

$$e + w = \frac{\sin\left(\theta_e + \theta_p\right)}{\cos\theta_e}\left(\frac{L}{2} - l_p\right) \tag{15}$$

where θ_e and θ_p are the rotation due to the initial imperfection and rotation after applying the axial load (p), respectively. All rotations are assumed formed by a uniform distribution of curvature over the plastic hinge length (l_p). The rotations are calculated by

$$\theta_e = \phi_e l_p = \tan^{-1}\left(\frac{e}{L/2 - l_p}\right) \tag{16}$$

$$\theta_p = \phi_p l_p \tag{17}$$

where ϕ_e and ϕ_p are the curvature due to the initial imperfection and after applying the axial load (p), respectively. It can be noticed that the plastic hinge length value is maintained unchanged along the entire loading procedure.

Giving the fixed rotational condition at both ends and the force distribution, maximum moments (absolute values) are obtained at both ends (symmetry) and bar mid-length. To maintain symmetry for a homogeneous bar, four plastic hinges are placed at maximum moment locations. It is assumed that such plastic hinges concentrate all deformations.

For the vertical displacement (v), it is assumed that deformation due to axial strain (ε) and curvature (ϕ) can be decoupled in the terms v_ε and v_ϕ, which are associated to the axial strain (ε) and curvature (ϕ), respectively, which simplifies the numerical procedure. Thus, the vertical displacement is determined by

$$v = v_\phi + v_\varepsilon = \left(L - 2l_p\right)\left[1 - \frac{\cos\left(\theta_e + \theta_p\right)}{\cos\theta_e}\right] + 4l_p\varepsilon_p \tag{18}$$

where ε_p is the axial strain at the plastic hinge region.

Thus, the engineering average axial stress ($\bar{\sigma}$) and average axial strain ($\bar{\varepsilon}$) are determined by

$$\bar{\sigma} = \frac{p}{\sum_i A_i} = \frac{p}{A} \tag{19}$$

$$\bar{\varepsilon} = \frac{v}{L} \tag{20}$$

The present study validates a plastic hinge formulation capable of reproducing the average axial stress versus average axial strain response of reinforcing bar with an initial imperfection under compression. The methodology, although described and compared to experimental evidence on isolated reinforcing bars, can be used to study column performance. Two different approaches from the literature could be adopted to obtain moment versus curvature responses: the Gomes and Appleton [**5**] formulation and the Bayrak and Sheikh [**11**] formulation. Gomes and Appleton [**5**] developed a stress versus

strain constitutive law for reinforcement under compression incorporating bar buckling as three plastic hinges that form once spalling of cover concrete occurs. The plastic hinges are defined based on fully plasticized cross-sectional area. The compressive constitutive law for the reinforcement is then applied into a sectional analysis by limiting the cyclic response that would be obtained if no buckling is present. Thus, an identical procedure can be followed, replacing the compressive envelop for the longitudinal bar with the proposed approach. Bayrak and Sheikh [**11**] followed a different direction. In their formulation experimental stress versus strain responses for reinforcing bar affected by buckling are used to predict sectional response. In this case, initiation of bar buckling occurs after spalling of cover concrete. At that point, ties are strained and confined concrete tends to push and bend the longitudinal reinforcement between ties outwards. The acting transverse force on the longitudinal reinforcement generates a midheight deflection, calculated base on an assumed shape function for the force distribution along the bar. The midheight deflection is set as the initial imperfection assuming that further actions are controlled by the axial force. Thus, an identical procedure can be followed, replacing the compressive envelop for the longitudinal bar with the proposed approach for a predefine imperfection.

3.5 Numerical implementation

The previously described model concentrates all deformations in four plastic hinges without distinction between elastic or plastic deformations, and maintaining the plastic hinge length constant. This, although allows using the model even for the initial loading stages while the material remains elastic, introduces differences with a model that treats the

elastic deformation as part of the entire bar length, rather than just the plastic hinge region. It is shown, in a later section, that the overall model response presents good agreement with experimental results, revealing that the assumption of concentrating all deformation at the plastic hinges has little impact in the general behavior.

3.5.1 Initial imperfection

The numerical procedure that includes the initial imperfection is described in **Fig. 8**. The model has one iterative scheme over one variable: the initial curvature (ϕ_1), that is, the curvature required to induce deformation in the bar by the externally applied load. Defined the initial curvature, and evaluated at the fiber and section levels, the curvature obtained after unloading is set as the curvature (ϕ_e), that once the externally applied load is removed, results in a permanent mid-length transversal deformation e.

An alternative scheme (Alternative 1, see **Fig. 8**) is also presented to guarantee force equilibrium in the axial direction. Using a zero axial strain would result in a small axial force, due to the asymmetry of the material model in tension and compression, which has little impact in the overall response. Incorporating the axial strain can be done in the same numerical schemes by adding this new variable. Most nonlinear numerical procedures can be used to solve the problem, such as Newton-Raphson, bisection method, etc.

The specimens that presented no initial imperfection can be treated as bars with small imperfections in order to observe buckling (with transversal displacement), which deviates

from the trivial solution that basically reproduces the compressive constitutive material response with signs of only axial displacement.

3.5.2 Application of axial force

The numerical procedure that applies the incremental axial force is described in **Fig. 9**. The scheme allows incrementally determining different loading stages by increasing the average axial strain ($\bar{\varepsilon}$) in the bar. The new strain value results in a new equilibrium, which is solved iteratively. The model has one iterative scheme over one variable: the additional curvature (ϕ_p), that is, the additional curvature induced in the bar by the axial load, which already has the imperfection included. As in the previous section, most nonlinear numerical procedures can be used to solve the problem.

4. MODEL CORRELATION WITH TEST RESULTS

The following section includes a comparison between the described model and experimental results from the literature.

4.1 Overview of tests

A series of tests carried out by Bayrak and Sheikh [**11**] are considered for comparison with the described model. The test program considered two important characteristics that made it suitable for the numerical comparison. The test program included different imperfection magnitudes and the tensile coupon tests were strained beyond the peak stress point. The experimental program carried out by Bayrak and Sheikh [**11**] was performed

using Grade 400 ($f_{y,nominal}$ = 400 MPa) 20M (d = 19.5 mm) steel reinforcing bars. Seven different tie spacing to longitudinal bar diameter ratios L/d were used, starting from 4 and ending with 10. For each L/d ratio, four different levels of initial imperfection (e) were tested, with ratios e/d ranging from 0 to 0.3. Initial imperfections were introduced into the bars, which had the two ends restrained against rotation, by pushing at the middle length of the bar with an external force, yielding to the desirable initial imperfection-over-diameter ratio (**Fig. 10aA**). The axial displacement was measured by four linear variable differential traducers (**Fig. 10aB**). Companion specimens were tested to validate the repeatability of the tests.

4.2 Model results

The material model was calibrated to a monotonic response including the modification in the degrading zone. The strain concentration zone, once degrading occurred, was set as the diameter length, which is consistent with the assumption of plastic hinge length of one diameter considered for the bar buckling model (i.e., l_p=d). The fracture strain was determined according to Eq. (**2**) for a 50 mm gauge length. The experimental tensile, analytical tensile (with and without the post-peak correction) and compressive responses are depicted in **Fig. 10** in engineering coordinates. Tensile responses are shown until fracture is set, whereas the compressive response is not shown in full range to adopt a reasonable scale.

The numerical procedure is performed using the calibrated material model and the cyclic model described in previous sections, discretizing the cross-section in twenty fibers,

which showed to be enough refinement. The average stress versus average strain response is compared to the experimental data in **Fig. 11**. All cases with different imperfection values are considered, and the numerical procedure adopted did not consider Alternative 1 (see **Fig. 8**), that is, no axial force equilibrium is guaranteed ($p \neq 0$). In order to numerically obtain the buckling response for bars with no imperfection a small perturbation was imposed. In this case, an imperfection-to-diameter ratio of 0.01 was used (i.e. $e/d=0.01>0$). Regarding the length-to-diameter ratio (L/d) only four values were considered for comparison: 4, 6, 8 and 10.

Fig. 11 shows reasonable good correlation for most cases. The peak capacity is better captured in the cases with lower imperfections. Differences are usually in the range from 5 to 15% when comparing the peak stress between the model and experimental results. Only the specimen with the largest imperfection and lowest length, i.e., $e/d=0.3$ and $L/d=4$, presents an analytical peak stress at a large strain, whereas the experimental result has already degraded presenting large differences. The post-peak response recovers the shape observed in the experiments. Differences are observed for specimens with low length-to-diameter ratio (e.g., $L/d=4,6$); where the model overestimates the stress, since it presents a less pronounced degradation than the tests. In the cases with relatively larger length-to-diameter ratio (e.g., $L/d=8,10$), the post-peak differences are usually less than 10% when comparing the stress between the model and experimental results, all the way up to the maximum experimental average axial strain commonly in the range between 20% and 30%. Regarding the overall response for different imperfection values introduced in the specimens, the analytical prediction reveals similar trends as the experimental response,

that is, the larger the imperfection the softer the response (lower stress). This is also consistent with other authors observations (e.g., Bae et al. [**13**]), which indicates that imperfection influences the bar response.

Additional comparison analyses were performed to establish the relevance of guarantying axial force equilibrium during the imperfection induction process. Equilibrium of the axial force for that stage was included as described in **Fig. 8** as Alternative 1. As expected, due to the flexural nature of the loading condition, the impact of such consideration was minor. **Fig. 12** includes a similar comparison as **Fig. 11**, for two representative cases: with an imperfection-to-diameter ratio of 0 (the nominal 0 value was an actual value of 0.01) and 0.3 (extreme cases). In this case, the additional dashed curves considered the correct equilibrium. As it can be seen, the response are almost identical, especially for the case with a low imperfection value (e/d=0). The largest difference is seen for the case with the largest imperfection value (e/d=0.3) and the smallest bar length value (L/d=4), where the maximum axial average stress does not differ in more than 2% to the case that does not satisfy initial axial force equilibrium, yielding to a response closer to the experimental data. Another difference, which is expected due to the nature of the implementation, is the initial stress value. The model without Alternative 1 (not satisfying initial axial force equilibrium) presents initial axial stresses, which are small for the case with a low imperfection value (e/d=0), and increase for the case with the largest imperfection value (e/d=0.3) and the smallest bar length value (L/d=4), where the initial stress value does not exceed the maximum axial average stress in more than 3%.

5. SUMMARY AND CONCLUSIONS

A model capable of representing the buckling of longitudinal reinforcing bars with induced initial imperfections was developed and compared to available experimental data. The model considers concentrated plasticity at four plastic hinges. The locations of plastic hinge correspond to zones of maximum moment that occurs during the induction of the imperfection as well as the deformation due to the axial load. The imperfections were induced by clamping the bar ends and applying a transversal force yielding in a residual maximum transversal displacement. Once the imperfection is set, the axial load acts on the specimen maintaining both ends fixed, which results in a moment configuration that is consistent with the stage of induction of imperfection. Thus, the mechanical model is maintained, and a sectional analysis, based on uniaxial constitutive material laws for steel, is used. The monotonic tensile response is characterized by common parameters, but it is additionally considered the post-peak behavior in order to guarantee a good response of the model. Giving the little information on this aspect, a linear response is proposed and a correction of the ultimate or fracture strain is defined based on strain concentration at the necking zone of the bar. The monotonic compressive response is characterized based on the tensile curve, assuming that tensile and compressive responses are identical in the true or natural coordinates, except that the compressive response does not present fracture. The cyclic behavior of the steel material was based on a simple curve that incorporates the Bauschinger effect, which reasonable well agrees with cyclic bar tests with few cycles.

The model assumes that all deformations are concentrated at the plastic hinges, resulting in an approximation of the response in the elastic range. Although the approximation, comparisons of the model with experimental results reveal that peak capacity is well captured, as well as the post-peak response shape. Differences are observed basically with the peak capacity for specimens with high imperfection values, and with the shape of the post-peak response for specimens with low length-to-diameter ratio.

Additionally, it was also observed from the tests comparison that the numerical procedure that includes initial axial force equilibrium at the imperfection induction stage (indicated as Alternative 1) has a small impact in the overall response, especially for the case of low imperfection value.

REFERENCES

[1] Bresler B, Gilbert PH. Tie Requirements for Reinforced Concrete Columns. ACI Journal Proceedings 1961;58(11):555-570.

[2] Mau ST, El-Mabsout M. Inelastic Buckling of Reinforcing Bars. Journal of Engineering Mechanics 1989;115(1):1-17.

[3] Dhakal RP, Maekawa K. Modeling for Postyield Buckling of Reinforcement. Journal of Structural Engineering 2002;128(9):1139-1147.

[4] Monti G, Nuti C. Nonlinear Cyclic Behavior of Reinforcing Bars Including Buckling. Journal of Structural Engineering 1992;118(12):3268-3284.

[5] Gomes A, Appleton J. Nonlinear Cyclic Stress-Strain Relationship of Reinforcing Bars Including Buckling. Engineering Structures 1997;19(10):822–826.

[6] Restrepo JI. Advanced Seismic Design Course Notes. Department of Structural Engineering, University of California at San Diego 2007.

[7] Mander JB, Priestley MJN, Park R. Seismic Design of Bridge Piers. Department of Civil Engineering, University of Canterbury, Report 84-2, 1984, 483 pp.

[8] Dodd LL, Restrepo-Posada JI. Model for Predicting Cyclic Behavior of Reinforcing Steel. Journal of Structural Engineering 1995;121(3): 433-445.

[9] Menegotto M, Pinto PE. Method of Analysis for Cyclically Loaded Reinforced Concrete Plane Frames Including Changes in Geometry and Non-Elastic Behavior of Elements Under Combined Normal Force and Bending. Proceedings, IABSE Symposium, Lisbon, Portugal 1973.

[10] Chang GA, Mander JB. Seismic Energy Based Fatigue Damage Analysis of Bridge Columns: Part I – Evaluation of Seismic Capacity. Department of Civil Engineering, State University of New York at Buffalo, Technical Report NCEER-94-0006, 1994, 483 pp.

[11] Bayrak O, Sheikh SA. Plastic Hinge Analysis. Journal of Structural Engineering 2001;127(9):1092-1100.

[12] Bae S, Mieses AM, Bayrak O. Inelastic Buckling of Reinforcing Bars. Journal of Structural Engineering 2005;131(2):314-321.

[13] Bae S, Mieses AM, Bayrak O. Closure to “Inelastic Buckling of Reinforcing Bars” by Sungjin Bae, Alexa M. Mieses, and Oguzhan Bayrak. Journal of Structural Engineering 2008;134(8):1399-1402.

FIGURES

Figure 1 – Monotonic tensile constitutive material model for steel.

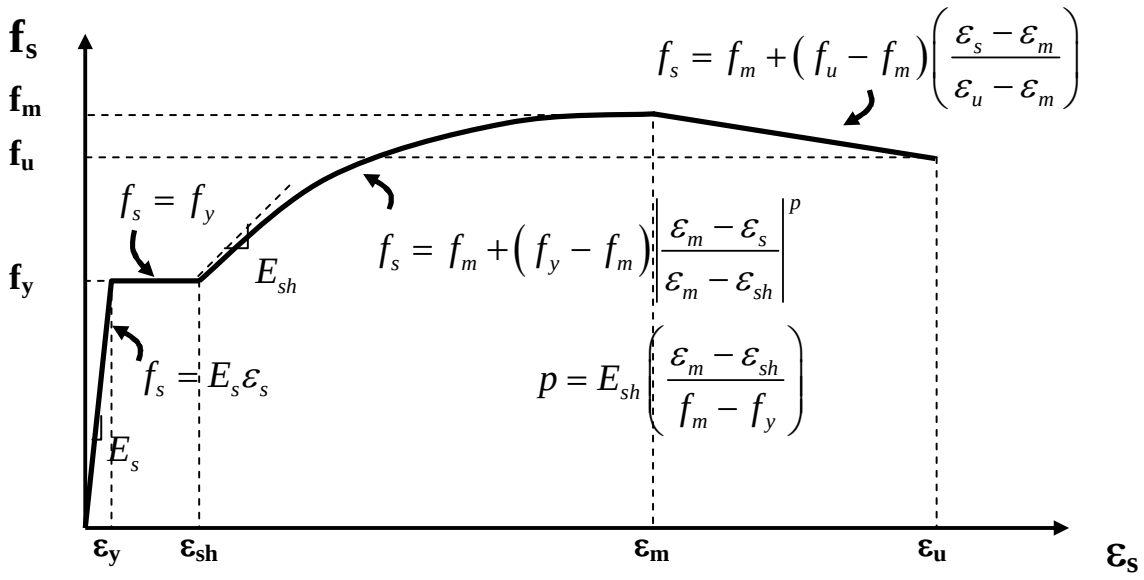

Figure 2 – Strain localization of reinforcing steel in tension.

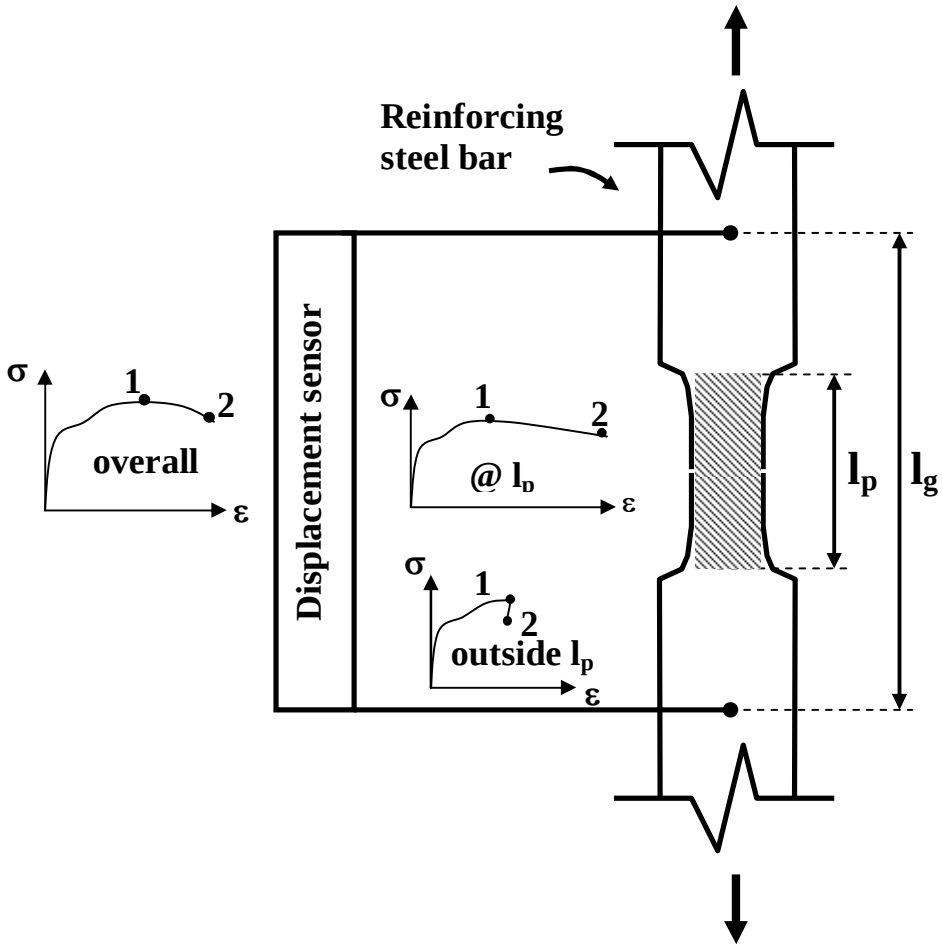

Figure 3 – Simple cyclic constitutive material model for steel.

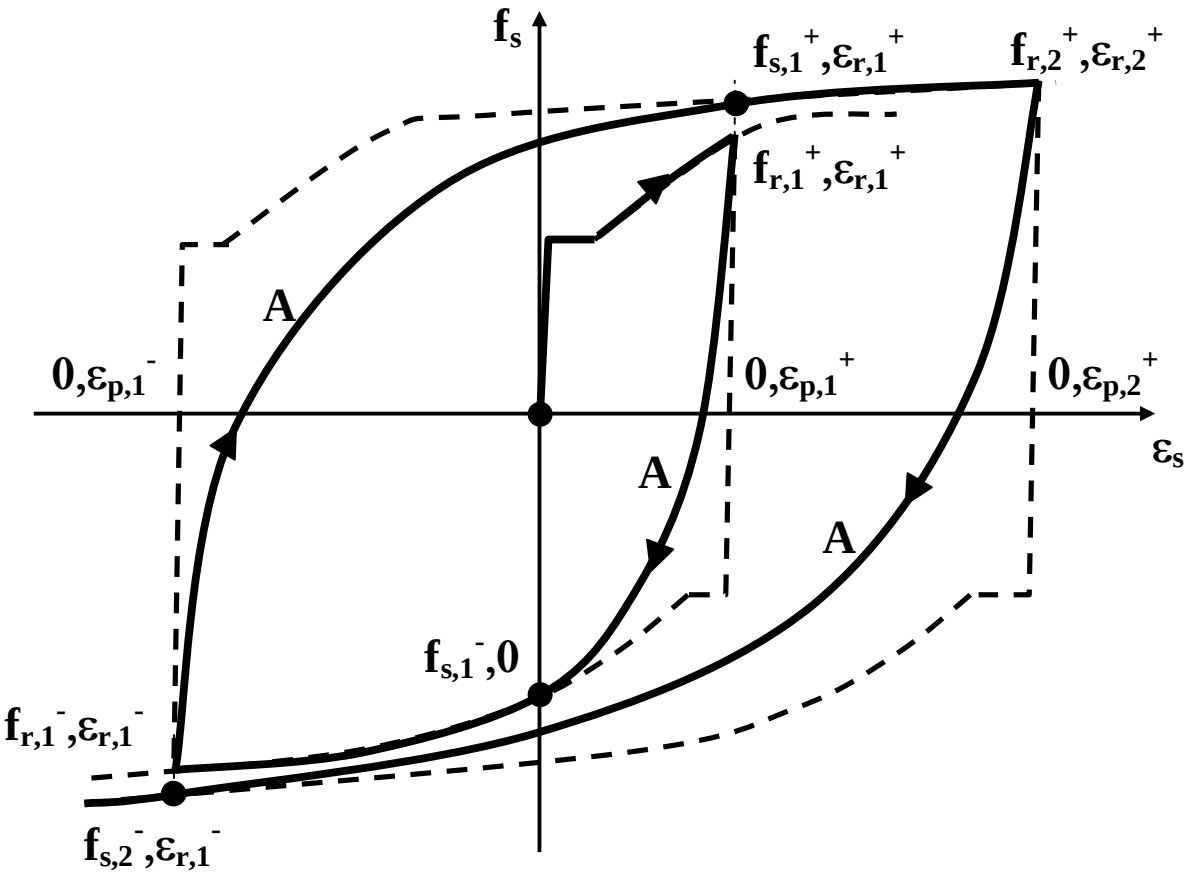

Figure 4 – Cyclic model comparison: (a) Kent and Park, 1973, specimen 8, (b) Ma, Bertero and Popov, 1976, specimen 1, and (c) Panthaki, 1991, specimen R5 (reported by Chang and Mander, 1994).

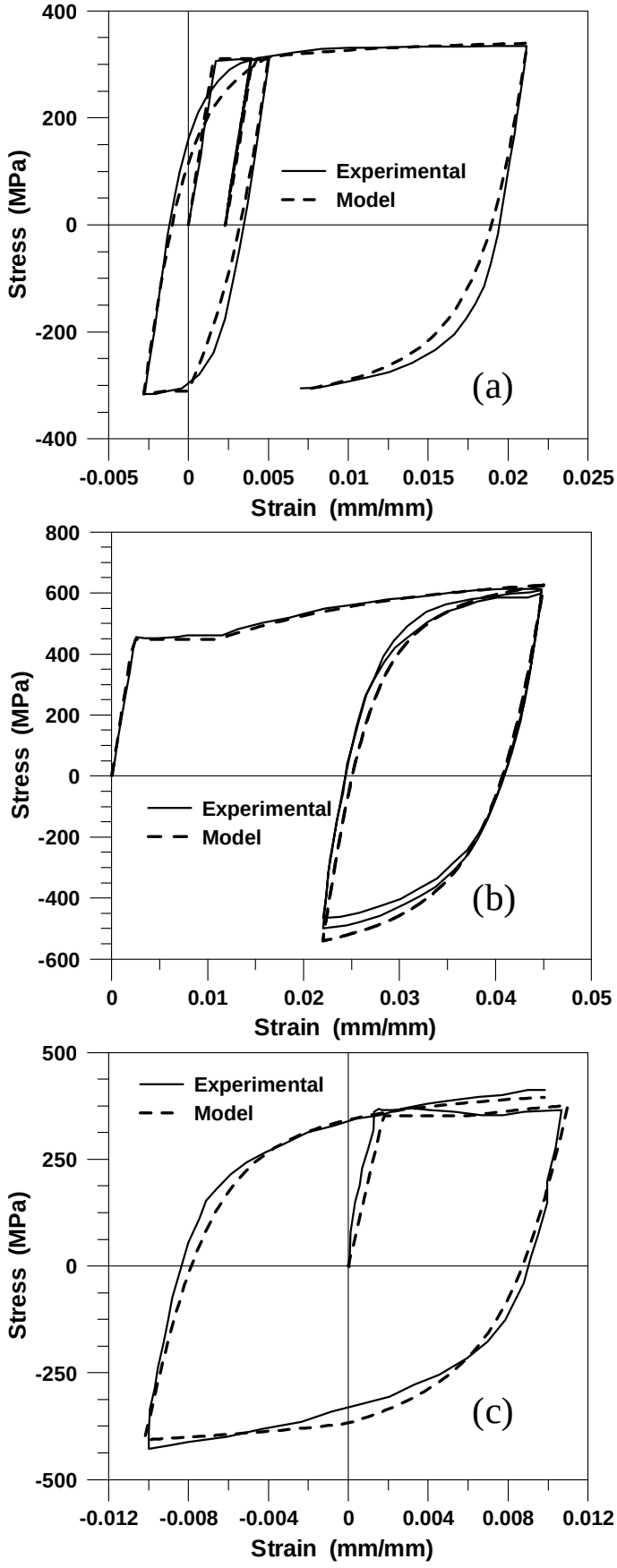

Figure 5 – Buckling representation of reinforcing bar with initial imperfection.

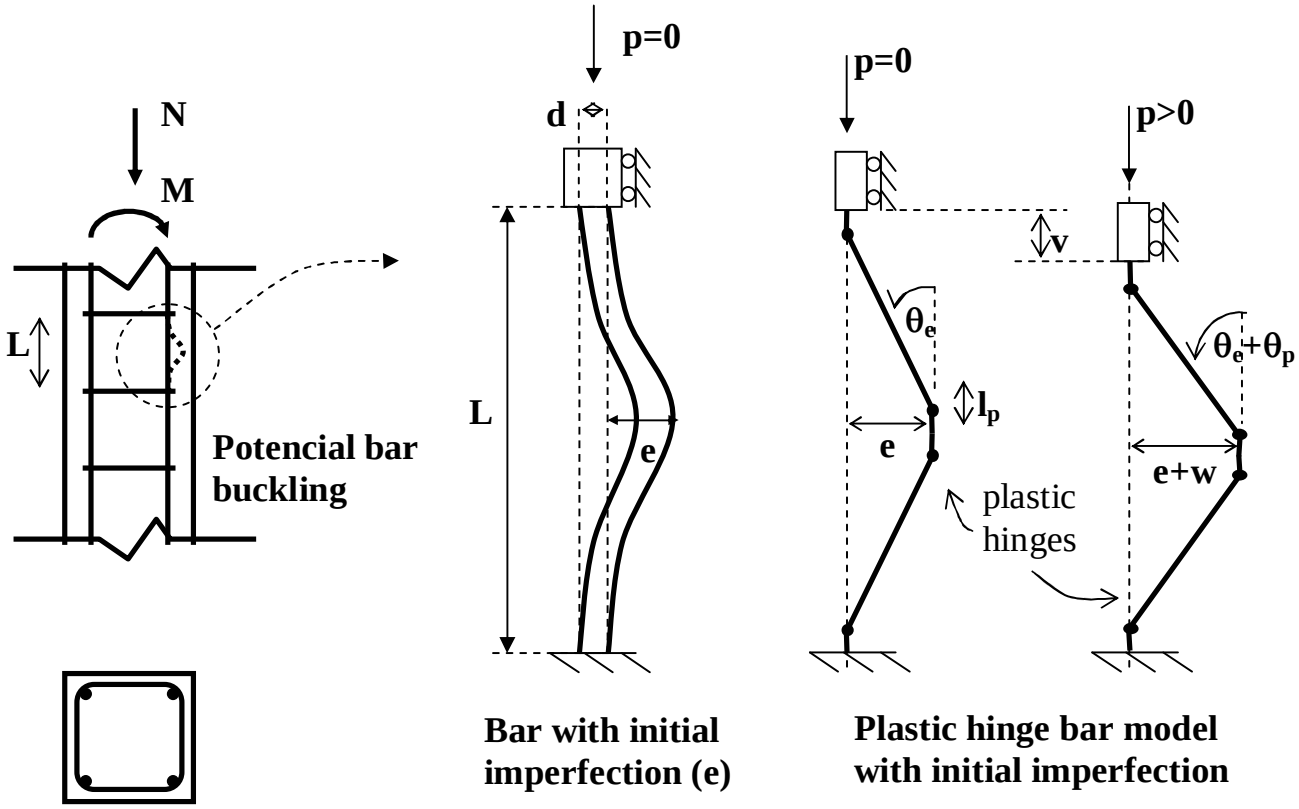

Figure 6 – Bar cross-section at plastic hinge zone: fiber discretization.

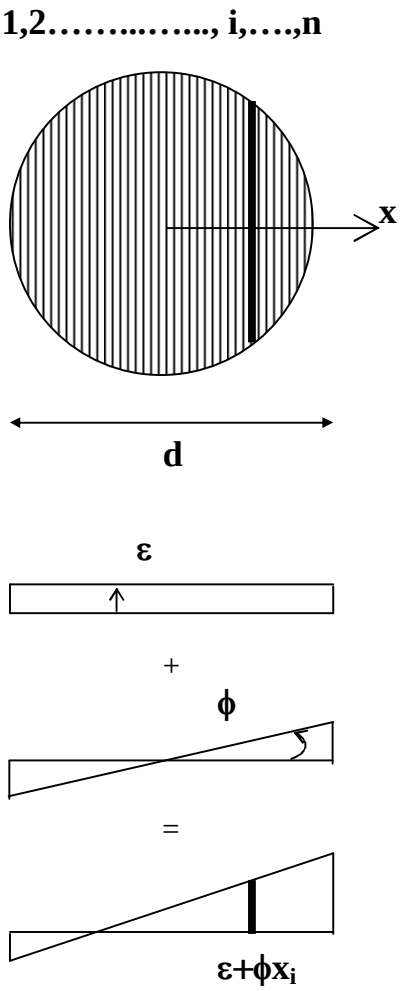

Figure 7 – Buckling plastic hinge model of reinforcing bar with initial imperfection (quarter bar).

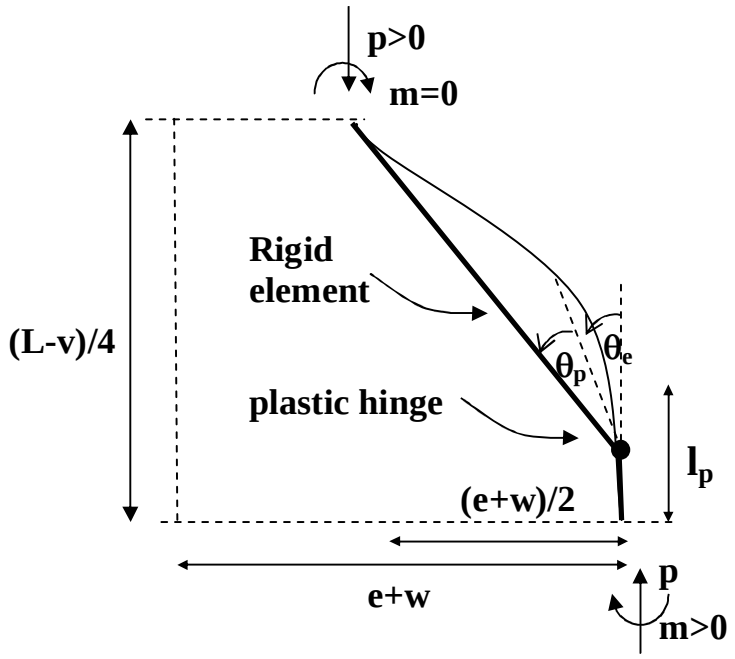

Figure 8 – Numerical procedure to impose initial imperfection to plastic hinge model.

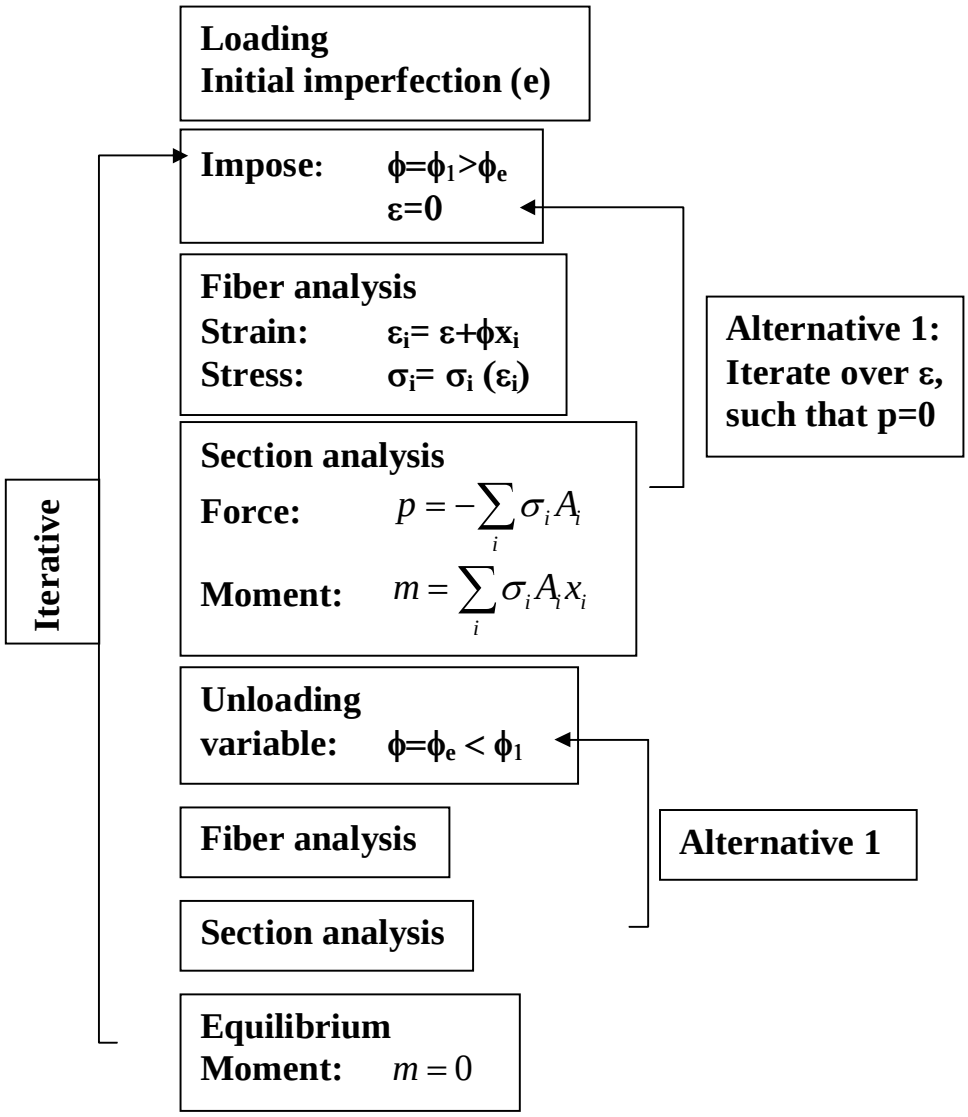

Figure 9 – Numerical procedure for buckling analysis of plastic hinge model.

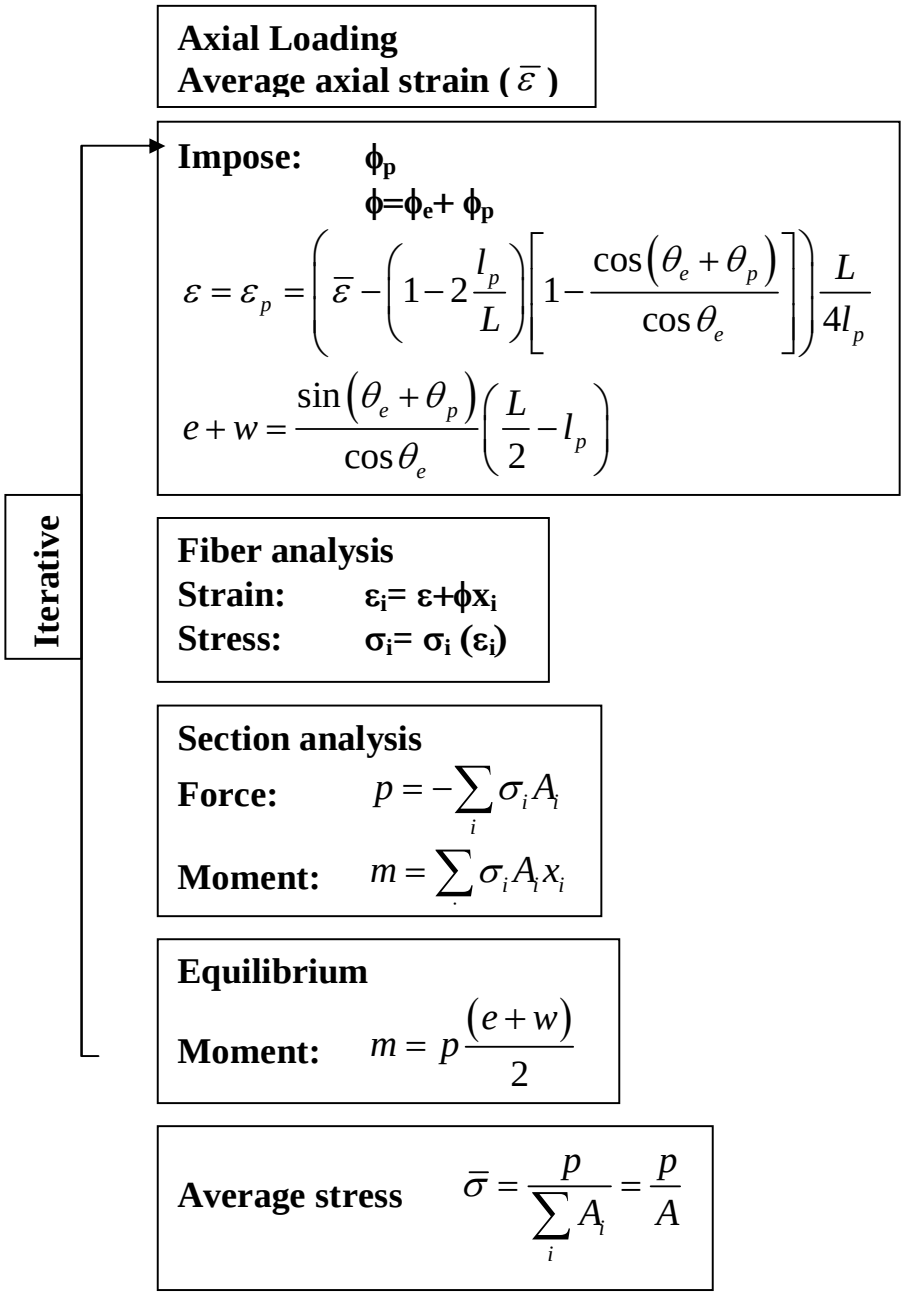

Figure 10B – Test setup scheme.

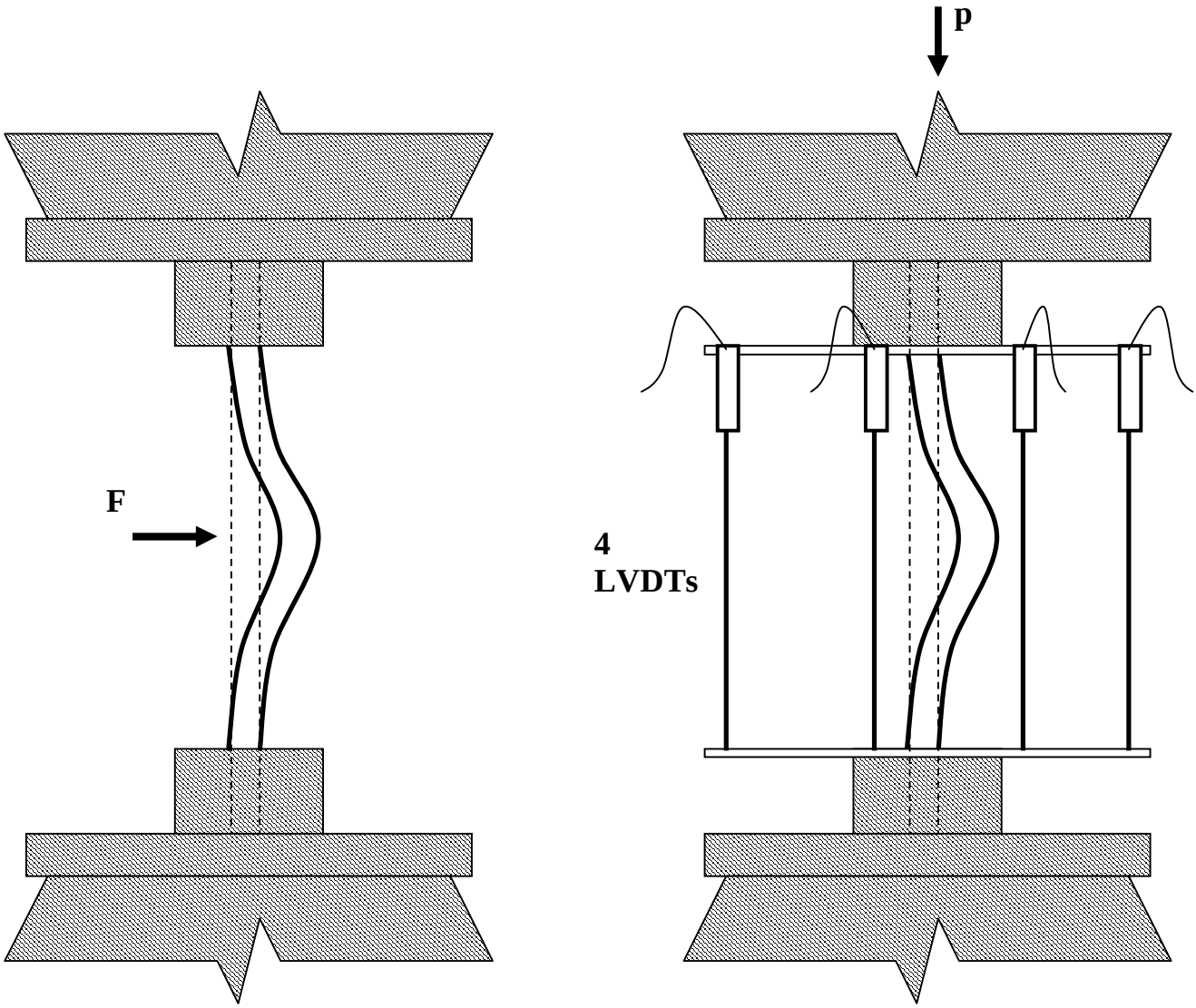

(a) Transversal deformation (initial imperfection)

(b) Axial deformation

Figure 10 – Stress – strain material calibration (tension and compression).

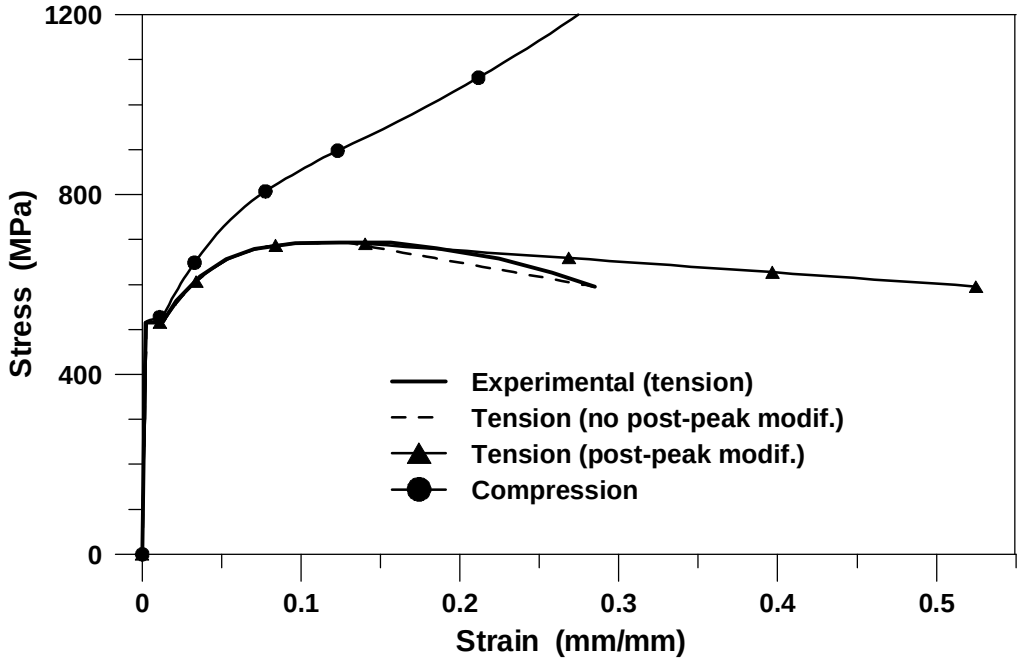

Figure 11 – Average stress – average strain bar buckling response: model without Alternative 1 (initial axial force equilibrium).

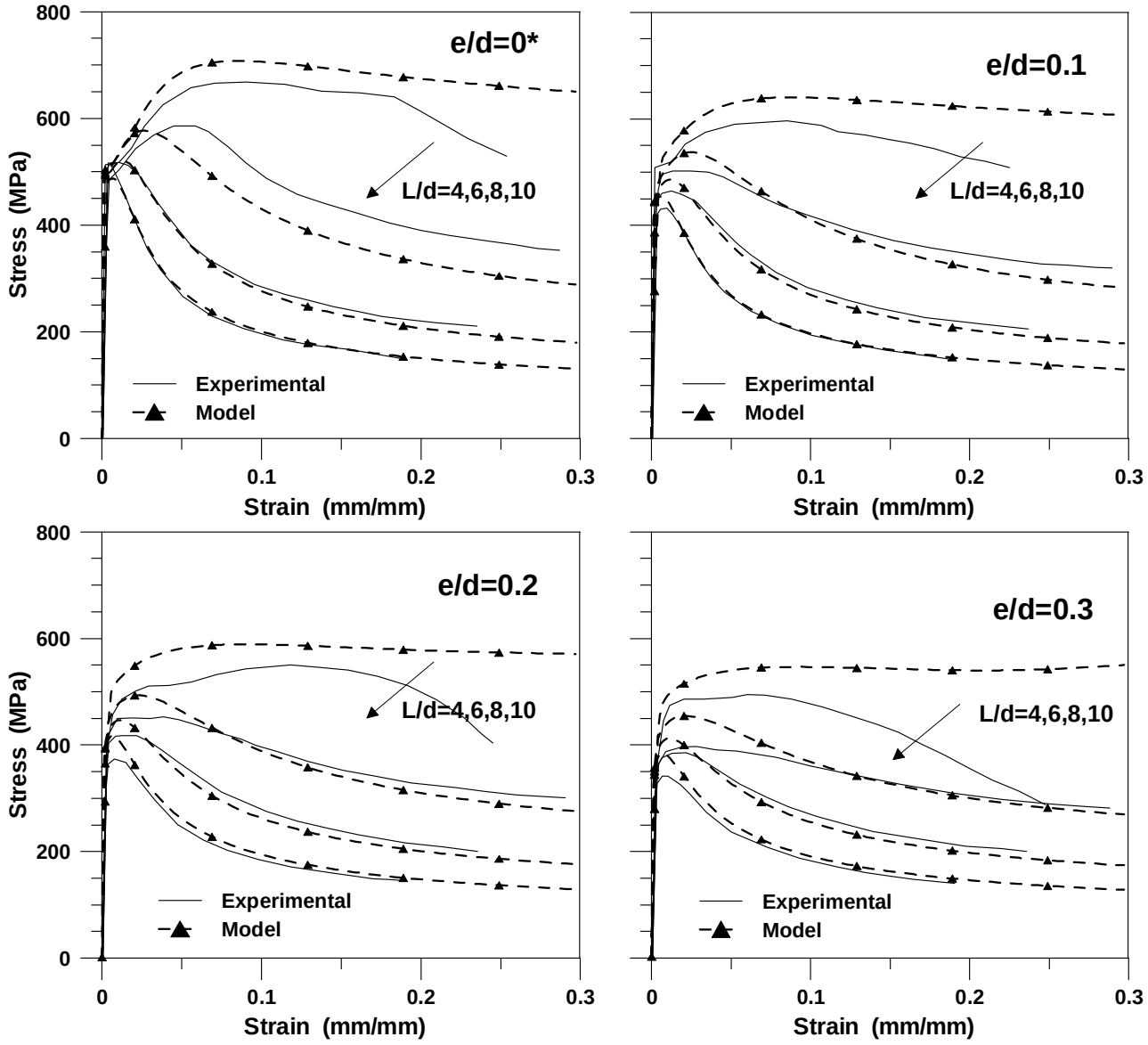

Figure 12 – Average stress – average strain bar buckling response: model with and without Alternative 1 (initial axial force equilibrium).